Influence of the thermomechanical processing on the fracture mechanisms of high strength aluminium/pure aluminium multilayer laminate materials

C.M. Cepeda-Jiménez[a]*, M. Pozuelo[b], O.A. Ruano[a], F. Carreño[a]

[a]*Departamento de Metalurgia Física, CENIM, CSIC, Av. Gregorio del Amo 8, 28040 Madrid, Spain*

[b]*Department of Materials Science and Engineering, 6531-G Boelter Hall, University of California, Los Angeles, CA 90095-1595, USA*

Abstract

The microstructure and mechanical properties, with emphasis in the impact fracture toughness behaviour, of two multilayer laminate materials have been investigated. The multilayer materials are constituted by alternated sheets of pure aluminium (Al 1200 or Al 1050) and high strength Al 7075 alloy. Stacked layers of these alloys have been successfully joined using two processing routes with different total hot rolling strains. Both laminates have been tested at room temperature under impact Charpy tests, 3-point bend tests and shear tests on the interfaces. Both laminates exhibited more than eight times improvement in impact fracture toughness over the monolithic Al 7075-T6. The toughness increase in the higher rolling strained laminate is almost entirely due to crack blunting mechanism, while in the lower strained laminate, crack deflection by delamination and crack renucleation processes were active.

Keywords: Multilayer aluminium structures; Interfacial strength; Fracture behaviour; Delamination; Hot roll-bonding

*Corresponding author. Tel.: +34 91 5538900; fax: +34 91 5347425.

E-mail address: cm.cepeda@cenim.csic.es (C.M. Cepeda-Jiménez)

1. Introduction

The need for low weight airframes has led to the development of very high-strength alloys used as plates, sheets and extrusions. The highest room temperature strengths attained in wrought aluminium alloy products correspond to the aluminium-zinc-magnesium-copper alloys [1]. However, the low fracture toughness limits the extensive application of this commercial heat-treatable aluminium alloy, especially at low temperatures, where the damage tolerance of 7xxx-series alloys is limited.

Toughening mechanisms in materials can be broadly divided into two categories, intrinsic and extrinsic. Intrinsic toughening implies inherent resistance of the microstructure to crack growth (grain size effects, precipitates, particle spacing, etc). Extrinsic toughening is induced by the rest of mechanisms that reduce the local stress intensity at the crack tip, for instance delamination at the interfaces [2].

Reviews of the literature on ductile phase toughening suggests the potential of extrinsic toughening by laminates consisting of alternating layers of a discontinuously reinforced metal and a ductile metal [3-6]. In these materials, the thickness of the ductile metallic, named ligament, greatly influences toughness [7].

Hot rolling is capable of obtaining good bonds between metallic layers improving toughness while refining the microstructure [8-10]. The interfaces that may delaminate are responsible for the high impact and fracture resistance of the multilayer materials and contribute to increasing the extrinsic toughening by different mechanisms. Delaminations in the layers ahead of the crack tip result in a reduction and redistribution of the local stress [11]. In the case of ultrahigh carbon steel (UHCS) based laminated composites, it has been shown that interlayer delamination is the principal mechanism of crack arresting [12-14]. This process makes crack propagation through the composite very difficult.

It is our contention that the toughness of Al 7075 alloy can be enhanced by combining this alloy with pure aluminium in multilayer composite materials due to both intrinsic and extrinsic mechanisms. Since pure aluminium is exceptionally ductile, crack blunting may occur within the aluminium layers, thus eliminating the need for layer delamination as a mechanism of crack arresting. This would represent an improved approach to toughening through lamination because it would reduce the need to control carefully the interface strength. Furthermore, since pure aluminium is relatively inexpensive compared to Al 7075 alloy, the multilayer system can be economically more attractive than monolithic Al 7075 alloy.

Therefore, the objective in this work is to obtain multilayer materials based on lightweight aluminium alloys by two roll bonding strain paths to optimize toughness. It is also to examine the combined effect of the constituent materials, the high strength of the Al 7075 alloy and the ductility of pure aluminium, on the main crack arrest mechanism.

2. Experimental procedure

2.1. Materials and processing

The aluminium alloys used in the present study were rolled Al 7075-T6 alloy (termed “D”) and commercial pure Al 1200-O (termed “G”) and Al 1050-H24 (termed “H”) sheets of 2 mm in thickness. The Al 7075 alloy was received in the T6 condition which is the strongest and most widely used form of this alloy. Samples of 60x120 mm^2 were used. The composition in atomic percentage of the alloys is included in **Table 1** and some mechanical properties are summarized in **Table 2**. The as-received sheets were cleaned with acetone. Two stacks of multilayer composites were considered. Eight layers of Al 7075 and seven layers of Al 1050 were stacked alternately, building a bundle of 30 mm in thickness and referenced in this work as ADH15. The second multilayer material was constituted by seven layers of pure Al 1200 and six layers of Al 7075 alloy stacked alternately to build a bundle of 26 mm in thickness and referenced as AGD13.

The two stacked aluminium materials were welded by Tungsten Inert Gas (TIG) at their edges to avoid oxygen penetration and delamination during processing, and then hot-rolled at 465 ºC in several passes without lubrication. This temperature was selected to be the solution temperature for the Al 7075 alloy (D). The rolls were 130 mm in diameter and the rolling speed was 334 mm/s. All rolling directions were parallel to the rolling direction of the as-received sheets.

After hot rolling, and due to the high temperatures employed during the processing, it was necessary to carry out a heat treatment to improve the mechanical properties of the Al 7075 alloy included in the laminated materials. The heat treatment that has been deemed optimal for the Al 7075 alloy is the T6 temper. This heat treatment involves solution treating the alloy at 465 ºC for 30 min, followed by rapid quenching in water and finally age hardening at 135 ºC for 14 h.

2.2. Microstructures

The microstructure at the bond interfaces in the L-T orientation was observed by scanning electron microscopy (SEM) using a JEOL JSM 6500F instrument with a field emission gun. The chemical compositions of the laminate interfaces were examined by an electron probe microanalyzer (Oxford Inca) operating at 15 kV. Metallographic preparation involved methods of standard surface preparation. The samples were electropolished in a 30% nitric acid solution in methanol at -20 ºC and 15 V.

2.3. Mechanical tests

2.3.1. Microhardness test

Microhardness measurements were made around the laminate interfaces with a Vickers indenter under loads of 10 g during 15 s.

2.3.2. Charpy test

Two mm V-notched Charpy type testing samples were machined with 10x10x55 mm^3 dimensions from as-received monolithic Al 7075 (D) alloy plates, pure aluminium plates of 10 mm in thickness with similar composition and mechanical characteristics than the Al 1200 (G) alloy, and ADH15 and AGD13 laminated materials. The samples were tested in the crack arrester orientation. The notch was machined to end at an individual layer of the test sample such that the crack front advances through each layer interface sequentially during the test. Charpy tests were conducted with a pendulum impact tester using a maximum capacity of 294 J. Three samples of each material were tested.

2.3.3. Three point bend test

The influence of the interfaces and the rolling strain on the mechanical properties of the two multilayer laminates was determined by the three point bend test, using notched charpy samples (10x10x55 mm^3) in the crack-arrester orientation. The stress, σ, and the strain, ε, were converted from the recorded raw data according to the following relations [15]:

$$\sigma=3pl/2ae^2 \qquad \varepsilon=6ed/l^2 \tag{1}$$

were *a* is the width of the sample, *e* the thickness, *l* the span length between the supports (40 mm), *p* the force applied on the sample and *d,* the midspan displacement of the sample.

The bend test was performed using a *Servosis* universal test machine under displacement control at a rate of 0.04 mm/s, with load and time recorded by the data acquisition program. At least two samples for each laminate were used to collect data. Fracture surfaces of selected samples were examined by both macroscopic analysis and scanning electron microscopy (SEM) to evaluate deformation micromechanims and any interlayer debonding.

2.3.4. Shear test

The bonding of aluminium surfaces is a crucial step in the present process. The interface strength was measured by shear tests in a universal test machine (cross-head speed of 0.005 mm/s) using samples of approximate dimensions 10x10x3 mm^3. The test was performed by clamping the sample between two metal supports. The interface to be tested is located just outside the border of the tool and parallel to the load direction. Then, a square punch at a given gap distance is used to apply the shear load until failure of the interface. The shear stress, τ, and the shear strain, γ, are given by the expressions [16]:

$$\tau=p/ae \qquad \gamma=\tan(\alpha)=d/l_{gap} \tag{2}$$

where *a*, *e*, *p* and *d* have been already defined, α is the shear angle and l_{gap} is the distance between the supports and the mobile punch, corresponding to 0.19 mm in this study.

Once the shear tests were carried out, the fracture surfaces were analyzed using SEM to asses more precisely the type of failure of the bonded layers.

3. Results and discussion

3.1. Processing

The multilayer laminates were processed by hot rolling at 465 ºC. Rolling was carried out in several series that have various number of passes of about 4-8% reduction per pass with the sample being reheated between series. **Figure 1** shows the processing schemes followed on each laminate. The total thickness reduction was $\in$=1.0 (corresponding to a reduction of about 2.7 to 1) for the ADH15 laminate and $\in$=0.8 (corresponding to a reduction of about 2.3 to 1) for the AGD13 laminate. After hot rolling, plates of about 11 mm in thickness, 260-320 mm in length and about 60 mm in width were obtained. The thickness of the aluminium layers was about 800 μm in the ADH15 laminate and about 920 μm in the AGD13 laminate.

3.2. Microstructure

The microstructure of the as-received Al 7075 rolled sheet in the “LT” orientation is presented in **Figure 2**. The as-received material shows large grains (10-20 μm) that are elongated and flattened parallel to the rolling direction. The insoluble iron-rich intermetallic particles and partially soluble constituent particles were observed to be randomly distributed. These intermetallic particles ranged in size from approximately 0.5 to 5 μm. The equilibrium precipitate $MgZn_2$, which is the main strengthening particle [17], was not observed in the SEM micrograph due to its small size. **Figure 3** shows the microstructure of the third interface in the ADH15 laminate and the second interface in the AGD13 laminate. The micrographs suggest a very good bond, although further assessment of the bond integrity requires quantitative mechanical testing. White and bright particles, identified as Al_2O_3 by microanalysis, are observed in the interface of both laminates. Compared with the ADH15 laminate, the alumina particles are more homogeneous and continuously distributed along the interfaces of the AGD13 laminate which was rolled to a lower strain. During rolling, the pure aluminium deforms plastically. In contrast, the alumina on the interface is brittle and its response to the stress is by fracturing. Therefore, during rolling, the alumina film is fractured and fragmented as a function of the rolling strain. The aluminium flowing between the

alumina particles is responsible of the bonding between clean metal surfaces. Therefore, the final interfaces are made up of oxide fragments and newly generated fresh areas of extruded aluminium. The size of these areas should increase with increasing deformation. These new areas of extruded aluminium will favour the diffusion of elements and the bond degree.

On the other hand, after rolling the microstructure of the Al 7075 (D) alloy in the laminates consists of elongated bands and grains finer than 2-3 μm. The change in shape and grain size with different total rolling strain is not noticeable, being slightly more homogeneous in the ADH15 laminate, which is the most strained.

Furthermore, the photomicrographs of **Fig. 3** show the presence of a interdiffusion band at the interfaces of both laminates which is extended to at least 20 μm into the pure aluminium layer (G or H). Microanalysis corresponding to a region close to the interface of the two laminates (**Figure 4**) shows concentration gradients that are attributed to diffusion of elements due to the high temperature and pressure during processing. The extent of the element (Zn and Mg) diffusion increases as the rolling strain increases (is higher in the ADH15 laminate). However, the morphology of the grains in the pure aluminium layers (G or H) seems to be very similar.

The diffusion of elements, which favours a possible precipitation, together with the localized strain around the interface, is expected to affect the thermal stability of the deformed material by a delay in recrystallization. Therefore, although the laminate materials were kept to high temperatures during processing and subsequent heat treatment, small size grains have been obtained in the D material, and in the G or H materials close to the interface.

3.3. Mechanical tests

3.3.1. Microhardness test

Microhardness measurements were carried out across the laminate interfaces (**Figure 5**). The increase in rolling strain (ADH15) followed a similar trend than that observed in the microanalysis (**Figure 4**). **Figure 5** shows that the gradient of elements across the interface causes a decrease in microhardness values, being this gradient slightly lower for the ADH15 (higher rolling strain). The variation in microhardness around the interface is more pronounced in the pure aluminium (G or H) than in the Al 7075 (D) for both laminates. This is attributed to the diffusion of elements across the interface, which helps pinning grain boundaries created during the rolling processing. This favours a finer microstructure in the pure aluminium towards the interfaces, increasing further the hardness.

3.3.2. Charpy test

The results of the Charpy impact test at room temperature are reported in **Table 3**. The two laminate materials were tested in the crack arrester orientation. The Charpy V-notched (CVN) energy average value for the monolithic Al 7075 (D) was 62 kJ/m^2, while for the monolithic pure aluminium was 912 kJ/m^2. The two laminate materials possess significantly higher impact energy than the monolithic Al 7075 alloy, more than eight times. Additionally, the impact value of the AGD13 laminate is 12.5% higher than that of the ADH15 laminate. Macrographs of Charpy tested samples for both laminates show different fracture behaviour, which will be analyzed in depth by the three point bend test. This difference in behaviour is related to the different distribution of alumina particles in the interfaces of the AGD13 laminate observed by SEM, which makes the bonding between layers more difficult, contributing to a possible delamination. On the other hand, a lower absorbed energy value in the high strain processed laminate (ADH15) can be attributed to a stronger interlayer bond.

3.3.3. Three point bend test

In order to understand the fracture mechanisms responsible for the high toughness, the laminates were tested in three point bending. This test allows a precise knowledge of the crack propagation, including a possible crack arrest at the interface, as well as the presence of interface debonding and crack renucleation in the next layer. Furthermore, this test permits comparison of toughness values by comparison of the areas inside the σ-ε curves. **Figure 6** shows stress-strain curves for the monolithic as-received alloys and processed laminates in the arrester orientation. The Al 7075 alloy presents a high bending stress of 960 MPa and low ductility. In contrast, the pure aluminium presents low strength (237 MPa) but excellent plasticity. High-integrity laminate materials have been obtained with a maximum bending stress of 600 MPa for the AGD13 laminate. The different maximum strength observed in the two materials is due to the notch position in the laminate, as well as to the different volume fraction of high strength Al 7075 alloy in each laminate.

One of the key features observed in the curves for both laminate materials is their improved ductility. At first sight, the bend curves for both materials show a similar pattern: a) a first load drop coincides with cracking of the first brittle layer until the crack is arrested at the interface with the ductile layer, and b) plateau regions that correspond to plastic deformation at the ductile aluminium until the next load drop occurs that indicates the critical strain needed for crack renucleation. However, the figure clearly reveals differences between the laminate materials. The curve corresponding to the AGD13 material shows load drops sharper than for the ADH15

laminate, which presents smooth drops in stress after cracking of the brittle layers, producing gradual crack arrest. On the other hand, the AGD13 laminate shows larger flat zones. The type of debonding observed in the AGD13 laminate does not damage the next layer, allowing a larger amount of deformation of the pure aluminium, thus favouring ductility. Therefore, the higher the extension of the plateau regions, the higher is the energy required to produce final failure, and the higher is the toughness.

Figure 7 shows macrographs of ADH15 and AGD13 samples after bend testing. The macrographs illustrate the high impact resistance of the laminate composites at room temperature. The AGD13 laminate presents several delaminations between blocks, which are constituted by two layers, together with extensive plastic deformation of the pure aluminium necessary to induce crack renucleation in the following layer. In contrast, no debonding is observed in the ADH15 laminate, despite extensive plastic strain of the pure aluminium layers. Furthermore, the cracks renucleated sequentially in adjoining layers. Therefore, the strong interfaces of the ADH15 laminate favours premature crack propagation. However, the samples show considerable ductility as evidenced by extensive necking in the layers. The type of failure obtained with the AGD13 and ADH15 laminates tested in bending at low strain rate is similar to that obtained in the Charpy test at high strain rate, showing no change in the operating deformation and fracture mechanisms as a function of strain rate.

Figure 8 shows fracture surfaces of the AGD13 and ADH15 laminates tested in bending in the arrester orientation. The analysis of the micrograph for the ADH15 sample (**Figure 8a** and **8c**) together with the previous macrograph (**Figure 7b**) shows that the cracks have propagated perpendicularly to the initial notch direction along the layers located above the notch due to the excellent bonding between the layers. Extensive plastic tearing of the Al alloy is observed in the ADH15 laminate, but without evidence of interface debonding. At this stage, deformation bands are apparent in the pure aluminium.

The micrograph of the AGD13 sample (**Figure 8b**) shows debonding of the aluminium layers, indicating crack deflection during bend testing. Macroscopically brittle failure is evident in the fast fractured region (D layers) of the AGD13 laminate. However, higher magnification observations of the D layers in both laminates (**Figure 8c** and **8d**) revealed ductile mechanisms like shallow dimples and voids distributed along the grain boundaries. Void coalescence at the grain boundary regions is a direct result of strain localization.

The bend test analysis of the two laminate materials reveals the existence of two fracture mechanisms, crack blunting in the ADH15 laminate and delamination in the AGD13 laminate at the pure aluminium layers. These mechanisms are responsible for

the enhanced fracture toughness and they can be controlled by the processing conditions. On the other hand, the sequence of events between crack arrest, plastic deformation and crack propagation is similar in both laminates. Although crack blunting in the ductile layer (clearly observed in the ADH15 laminate) prevents crack propagation, a crack opening stress still persists at the crack tip. This stress is large enough to continue the crack propagation in the subsequent layers after certain plastic deformation. On the contrary, the crack deflection observed in the AGD13 laminate due to a not-perfect bonding makes difficult crack nucleation in the next layer. The homogeneous band of alumina along the interface of the AGD13 laminate shown in SEM micrographs, which reduces the cohesion between the layers, facilitates debonding during the test, i.e. delamination of the composite.

3.3.4. Shear tests

To characterize precisely the mechanical properties of interfaces, which are responsible of the two fracture mechanisms observed (delamination and crack blunting), shear tests have been performed (**Figure 9**). Due to the high temperatures employed during the processing (welding, rolling and heat treatment), both pure aluminium alloys in the laminated materials show similar mechanical behaviour than the as-received Al 1200 (G) alloy. For simplification, only the Al 1200 alloy has been included in **Fig. 9**. The maximum shear stress of the Al 7075 (D) alloy is 287 MPa, showing low elongation to failure. In contrast, the maximum shear stress of pure aluminium is only 58 MPa, but it presents excellent ductility. In the description that follows, the interfaces are assigned numbers to indicate their location in the laminate (for example, i4 means interface four). The results for both laminates show that there is no difference between inside or outside interfaces, showing similar mechanical strength. The interfaces of the ADH15 laminate are ductile and have elongation-to-failure values somewhat higher than for the monolithic pure aluminium alloy due to the different heating conditions during processing. Failure occurred outside of the bond region in the Al 1050 (H) (ductile rupture in the Al adjacent to the interface), thus the bond strength exceeds the fracture strength of the weaker component, an indication of high bond integrity. On the contrary, the interfaces of the AGD13 laminate show a mixture failure, being initially ductile, with cohesive failure of the weaker component, Al 1200 (G), and finally failure along the interface between the layers in a catastrophic manner. Although these interfaces are less ductile, they present similar maximum stress than those of the ADH15 laminate.

Figure 10 shows SEM micrographs of the shear fracture surface of an interface in the AGD13 laminate. These micrographs show clearly the mixture failure obtained

during the shear test. This type of failure starts with a cohesive failure in the pure Al and is followed by a sudden failure at the interface. The upper side of the micrograph of **Figure 10a** corresponds to the plastic deformation in the Al 1200 (G). At the bottom of this figure and in **Figure 10b** at higher magnification, a dimple topography characteristic of microvoid coalescence in shear fracture mode is observed in the Al 7075 alloy.

The influence of rolling processing is clearly demonstrated in the behaviour of the AGD13 and ADH15 laminates. A more severe processing, with layers too well bonded, would be less adequate to obtain delamination and therefore a lower laminate toughness should be obtained. Thus, the interface behaviour observed in shear tests is totally in agreement with the previous mechanical tests (Charpy and bending) and their fractographs.

4. Conclusions

High-integrity bulk materials have been obtained by two effective roll-bonding processing ($\in$=1 or $\in$=0.8) conducted to improve the impact fracture toughness of Al 7075 alloy. Both laminates were found to exhibit more than eight times improvement in impact fracture toughness over monolithic Al 7075-T6. The results of mechanical behaviour of the two laminates considered reveal the importance of the ductility of the pure aluminium, which is capable of arresting cracks by two different fracture mechanisms.

The increase in toughness, of more than eight times in the ADH15 laminate (rolling strain, $\in$=1), is due to crack blunting, while in the AGD13 laminate (rolling strain, $\in$=0.8) crack deflection by delamination and crack renucleation processes were active increasing impact toughness by more than nine times. Therefore, improved toughness can be obtained by mean of extrinsic fracture mechanisms (delamination), if the interfaces bond is optimised by the processing.

The presence of an alumina layer at the interface determines the bond quality and therefore the mechanical properties of the laminates.

The occurrence of a stepped fracture surface in the laminate materials, in contrast to the catastrophic fracture of Al 7075 alloy, was observed under both slow strain rate loading conditions (three point bend tests) and high strain rate (impact) loading conditions (Charpy tests), showing no change in the fracture mechanisms as a function of strain rate.

Acknowledgements

Financial support from CICYT (Project MAT2003-01172) is gratefully acknowledged. C.M. Cepeda-Jiménez thanks the Spanish Ministry of Education and Science for a Juan de la Cierva contract. We also thank L. del Real-Alarcón for the welding work, F.F. González-Rodríguez for assistance during hot rolling and J. Chao-Hermida for assistance with the Charpy impact test.

References

[1] Aluminium. Properties and Physical Metallurgy, J.E. Hatch (Ed.), American Society for Metals, Ohio,1984.

[2] A. Rohatgi, D.J. Harach, K.S. Vecchio, K.P. Harvey, Acta Mater. 51 (2003) 2933-2957.

[3] D.R. Bloyer, K.T. Venkateswara-Rao, O.R. Ritchie, Mater. Sci. Eng. A239-240 (1997) 393-398.

[4] T. Li, F. Jiang, E.A. Olevsky, K.S. Vecchio, M.A. Meyers, Mater. Sci. Eng. A443 (2007) 1-15.

[5] D.R. Bloyer, K.T. Venkateswara-Rao, R.O. Ritchie, Mater. Sci. Eng. A216 (1996) 80-90.

[6] T. Li, F. Grignon, D.J. Benson, K.S. Vecchio, E.A. Olevsky, F. Jiang, A. Rohatgi, R.B. Schwarz, M.A. Meyers, Mater. Sci. Eng. A374 (2004) 10-26.

[7] T.M. Osman, J.J. Lewandowski, D.R. Lesuer, Mater. Sci. Eng. A229 (1997) 1-9.

[8] F. Carreño, J. Chao, M. Pozuelo, O.A. Ruano, Scripta Mater. 48 (2003) 1135-1140.

[9] M. Pozuelo, F. Carreño, O.A. Ruano, Mater. Sci. Forum 426 (2003) 883-888.

[10] M. Slámová, P. Homola, M. Karlík, Mater. Sci. Eng. A462 (2007) 106-110.

[11] D.R. Lesuer, C.K. Syn, O.D. Sherby, J. Wadsworth, J.J. Lewandowski, W.H. Hunt Jr, Int. Mater. Rev. 41 (5) (1996) 169-197.

[12] M. Pozuelo, F. Carreño, O.A. Ruano, Comp. Sci. and Tech. 66 (2006) 2671-2676.

[13] D.W. Kum, T. Oyama, J. Wadsworth, O.D. Sherby, J. Mech. Phys. 31 (1983) 173-186.

[14] Y. Ohashi, J. Wolfenstine, R. Koch, O.D. Sherby, Mater. Sci. Eng. A151 (1992) 37-44.

[15] C.F. Feng, L. Froyen, Acta Mater. 47 (1999) 4571-4583.

[16] G.E. Dieter, Mechanical Metallurgy, SI Metric, UK, 1988.

[17] F. Viana, A.M.P. Pinto, H.M.C. Santos, A.B. Lopes, J. Mater. Process. Tech. 92-93 (1999) 54-59.

Figure Captions

Figure 1. Scheme of the processing temperature of a) ADH15 laminate and b) AGD13 laminate.

Figure 2. SEM micrograph showing the microstructure of as-received Al 7075-T6 (D) alloy in the LT orientation.

Figure 3. SEM micrographs showing: a) interface 3 in ADH15; b) layer D7 in ADH15; c) interface 2 in AGD13; d) layer D6 in AGD13.

Figure 4. Atomic percentage of Zn and Mg as a function of the distance to the interface 2 in ADH15 and AGD13 laminates.

Figure 5. Vickers microhardness of the ADH15 and AGD13 laminates as a function of the distance to the interface 7.

Figure 6. Three point bend tests of as-received aluminium alloys and ADH15 and AGD13 laminates.

Figure 7. Macrographs of fractured samples from bend tests: a) AGD13; b) ADH15.

Figure 8. SEM micrographs showing fractures surfaces from bend tests: a) low magnification in ADH15; b) low magnification in AGD13; c) high magnification in layer D of ADH15; d) high magnification in layer D of AGD13. The white arrows indicate the crack propagation direction.

Figure 9. Shear tests at the interfaces of the ADH15 and AGD13 laminates compared with as-received aluminium alloys.

Figure 10. SEM micrographs showing fractured surfaces from shear tests of AGD13 laminates (Interface 7): a) low magnification; b) high magnification.

.

Table 1. Chemical composition of as-received aluminium alloys (atomic percent).

Alloy	**Si**	**Fe**	**Cu**	**Mn**	**Mg**	**Cr**	**Zn**	**Ti**
7075 “D”	0.14	0.06	0.60	<0.01	2.92	0.12	2.56	0.03
1050 “H”	0.12	0.21	<0.005	0.02	0.01	<0.010	<0.005	<0.010
1200 “G”	0.16	0.15	<0.005	<0.010	0.01	<0.010	<0.005	0.01

Table 2. Mechanical properties of as-received aluminium alloys. (UTS= ultimate tensile strength; YS= yield point; HV= Vickers Hardness; T6=solution treating followed by quenching and finally peak age hardening; H24=work hardening followed by partially annealing (240ºC); O=annealing followed by recrystallization)

Alloy	**UTS (*) (MPa)**	**YS (*) (MPa)**	**HV**	**Elongation (*) (%)**
7075-T6 “D”	545	475	188	8
1050-H24 “H”	105	75	44	10
1200-O “G”	90	40	29	40

(*) Data provided by the alloy maker from tensile tests

Table 3. Charpy V-notched (CVN) (kJ/m^2) energy of as-received and laminate materials.

Material	**CVN Energy (kJ/m^2)**
7075-T6 “D”	62
Pure aluminium (99%)*	912
ADH15	502
AGD13	565

*Result obtained from a plate of pure aluminium, 10mm in thickness

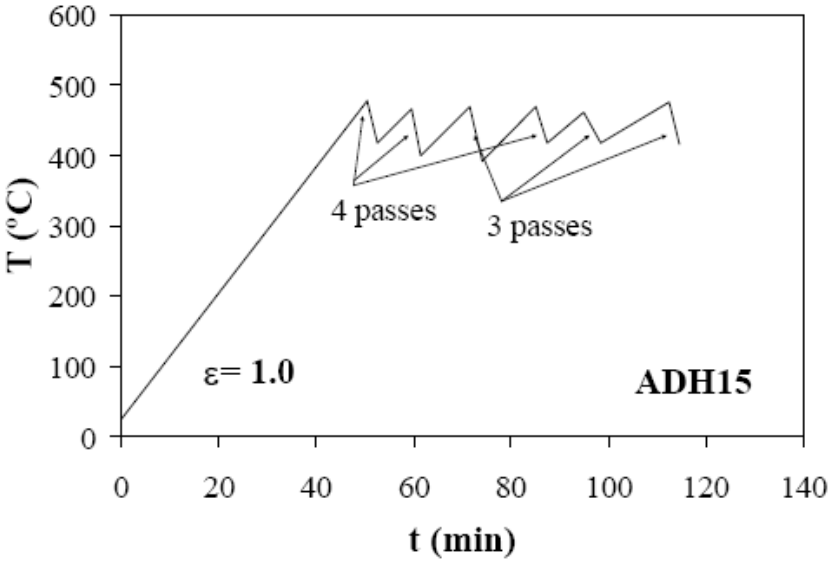

Figure 1a

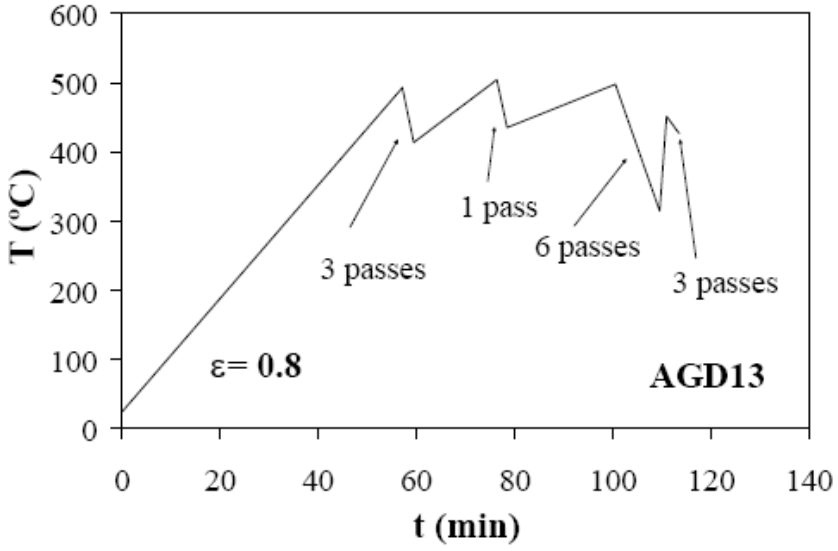

Figura 1b

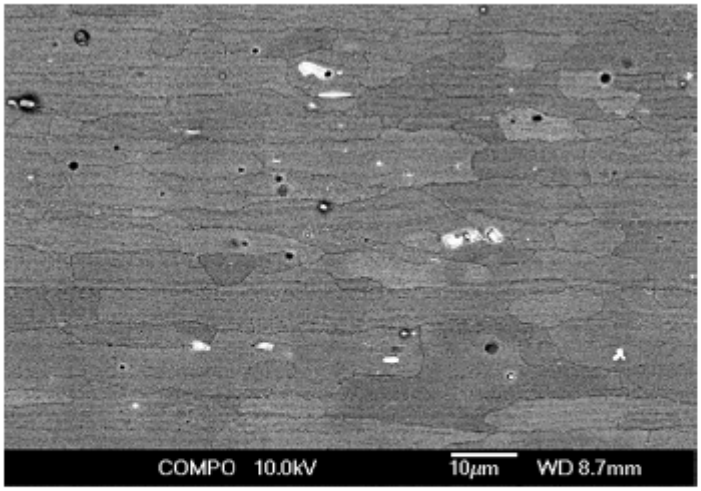

Figure 2

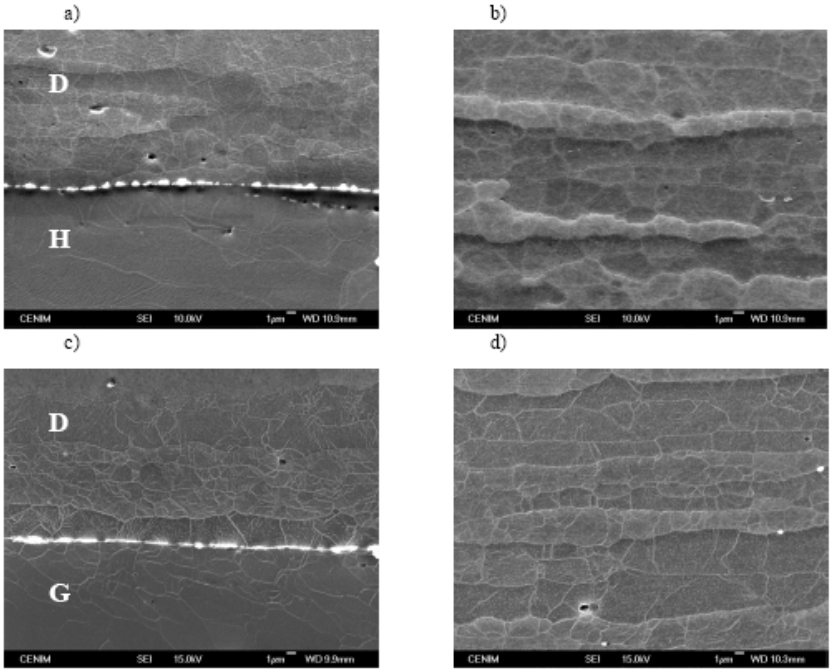

Figure 3

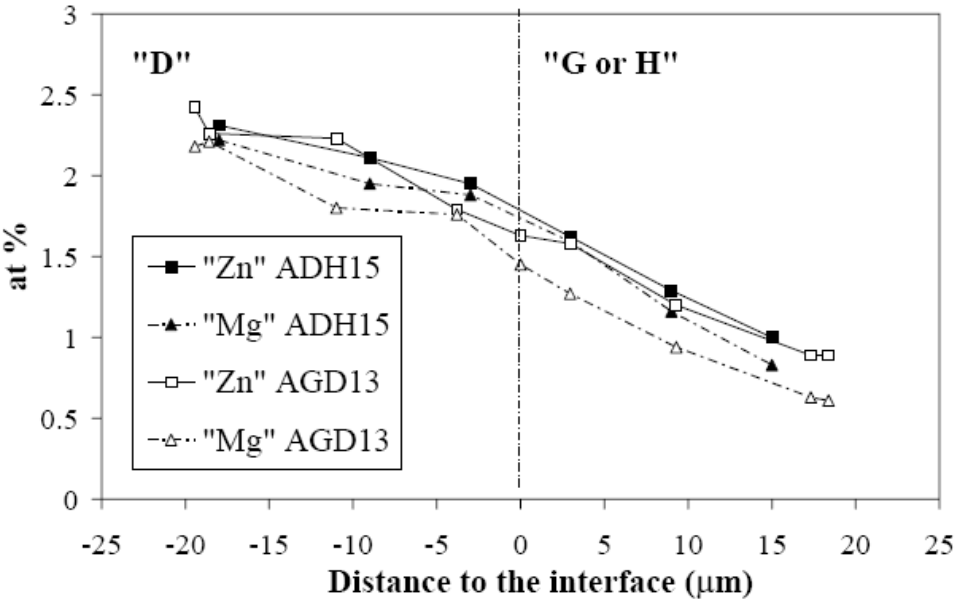

Figure 4

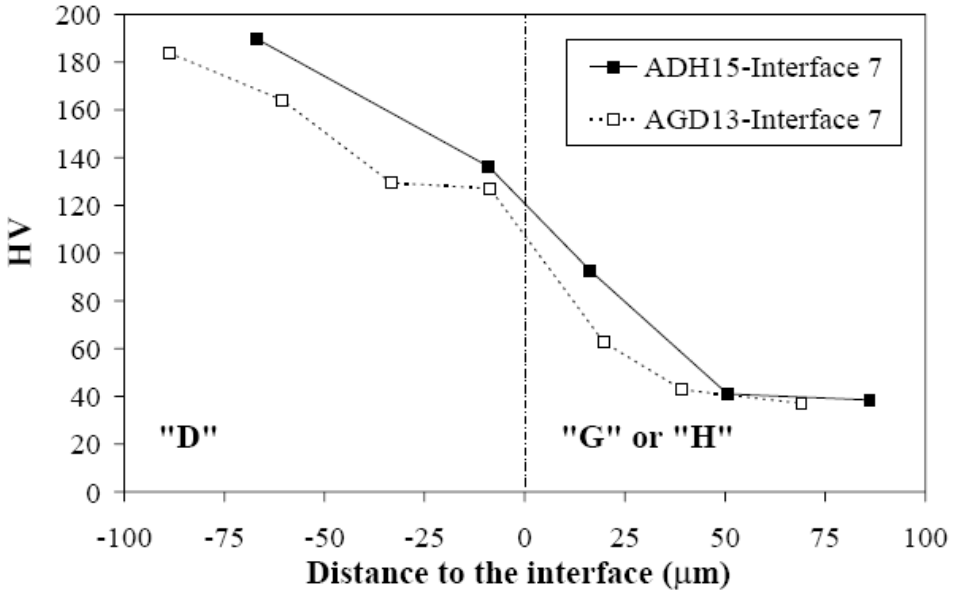

Figure 5

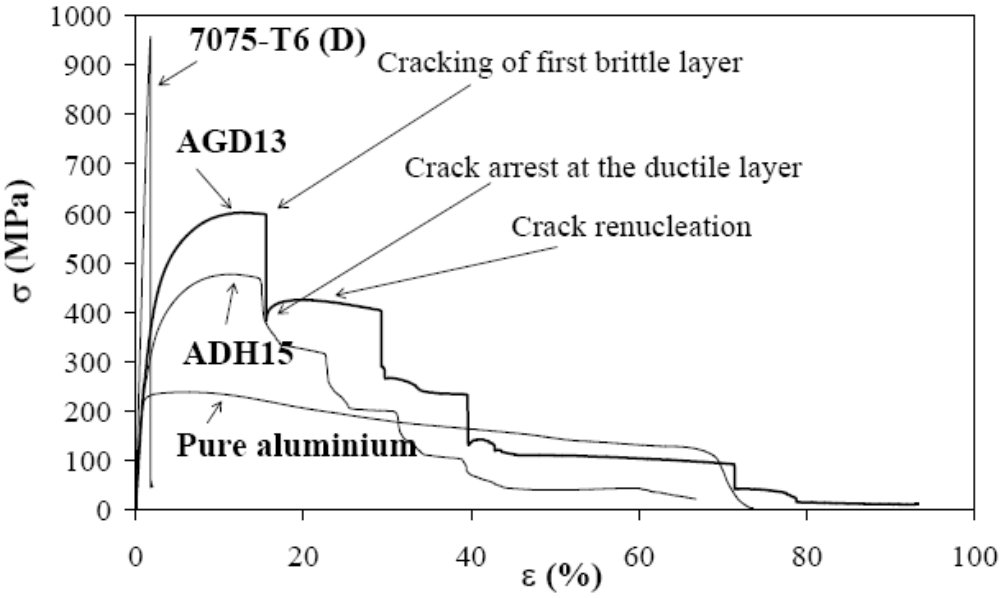

Figure 6

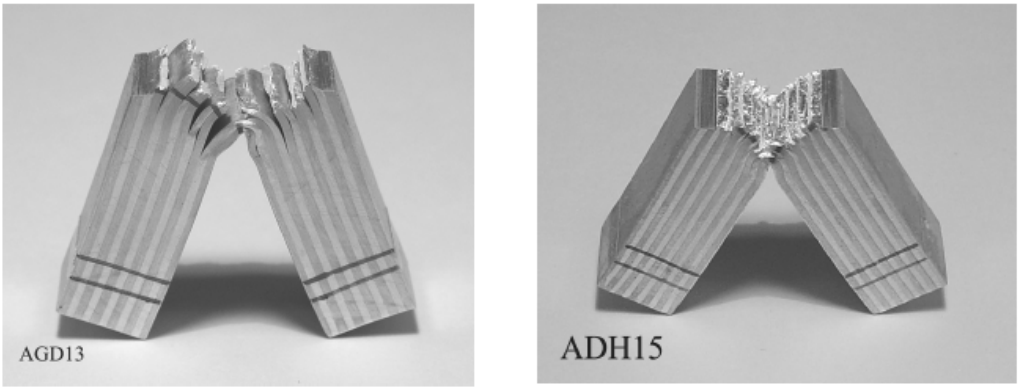

a) b)

Figure 7

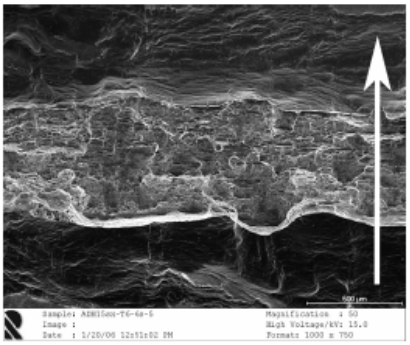

a)

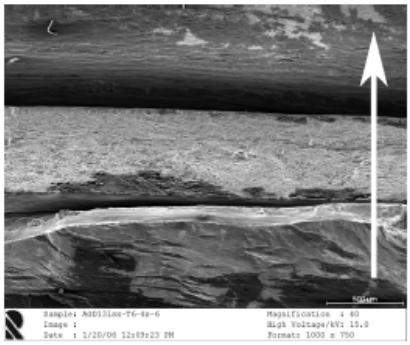

b)

Figure 8

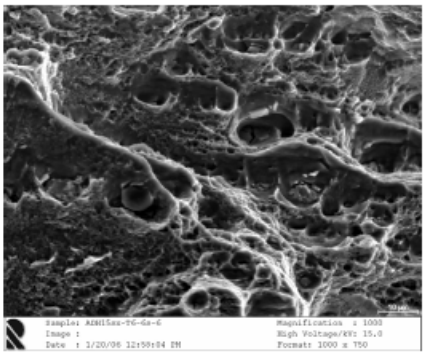

c)

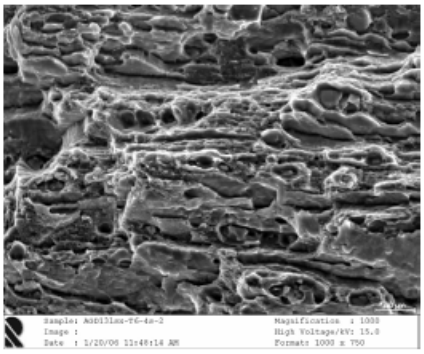

d)

Figure 8. (Continued)

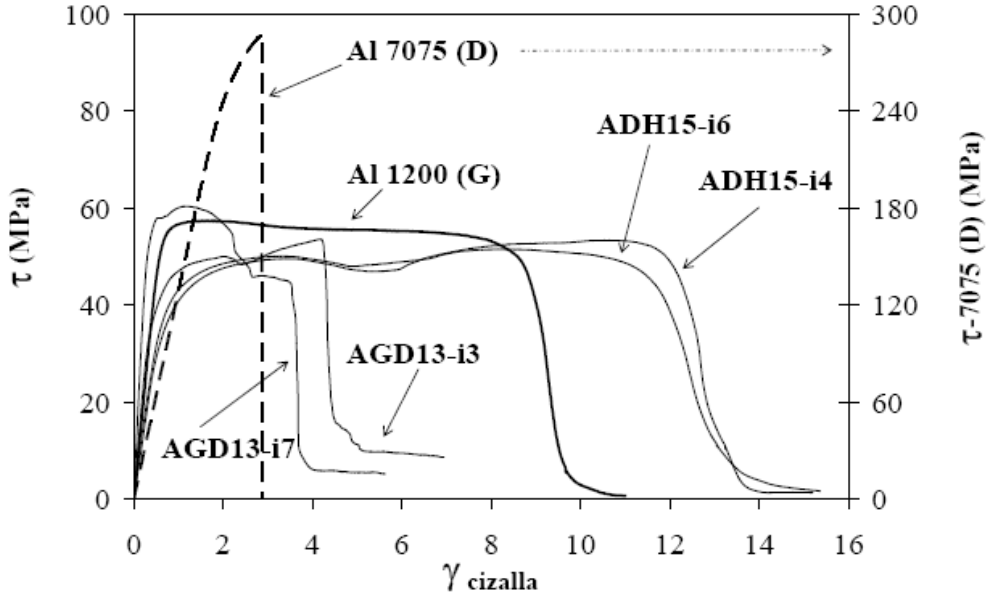

Figure 9

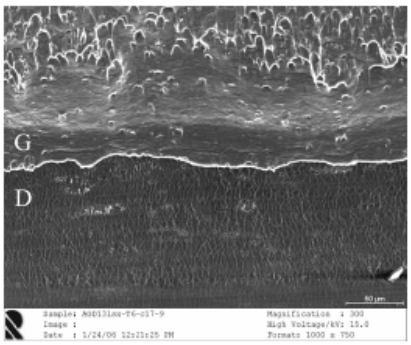

a)

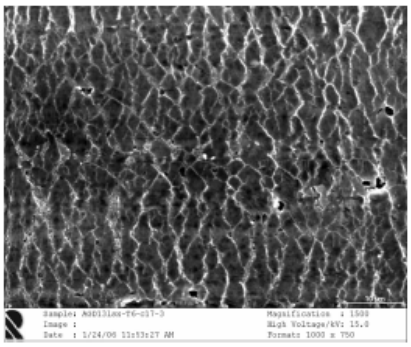

b)

Figure 10